

# Electron transfer across a thermal gradient

 Galen T. Craven<sup>a</sup> and Abraham Nitzan<sup>a,b,1</sup>
<sup>a</sup>Department of Chemistry, University of Pennsylvania, Philadelphia, PA 19104; and <sup>b</sup>School of Chemistry, Tel Aviv University, Tel Aviv 69978, Israel

This contribution is part of the special series of Inaugural Articles by members of the National Academy of Sciences elected in 2015.

Contributed by Abraham Nitzan, June 9, 2016 (sent for review May 4, 2016; reviewed by David M. Leitner and Marshall Newton)

**Charge transfer is a fundamental process that underlies a multitude of phenomena in chemistry and biology. Recent advances in observing and manipulating charge and heat transport at the nanoscale, and recently developed techniques for monitoring temperature at high temporal and spatial resolution, imply the need for considering electron transfer across thermal gradients. Here, a theory is developed for the rate of electron transfer and the associated heat transport between donor–acceptor pairs located at sites of different temperatures. To this end, through application of a generalized multidimensional transition state theory, the traditional Arrhenius picture of activation energy as a single point on a free energy surface is replaced with a bithermal property that is derived from statistical weighting over all configurations where the reactant and product states are equienergetic. The flow of energy associated with the electron transfer process is also examined, leading to relations between the rate of heat exchange among the donor and acceptor sites as functions of the temperature difference and the electronic driving bias. In particular, we find that an open electron transfer channel contributes to enhanced heat transport between sites even when they are in electronic equilibrium. The presented results provide a unified theory for charge transport and the associated heat conduction between sites at different temperatures.**

electron transfer | heat transfer | transition state theory | Marcus theory | thermal gradient

The study of electronic transport in molecular nanojunctions naturally involves consideration of inelastic transport, where the transporting electron can exchange energy with underlying nuclear motions (1, 2). Such studies have been motivated by the use of inelastic tunneling spectroscopy, and more recently Raman spectroscopy, as diagnostic tools on one hand, and by considerations of junction stability on the other. In parallel, there has been an increasing interest in vibrational heat transport in nanostructures and their interfaces with bulk substrates (3–11) focusing on structure–transport correlations (12–15), molecule–substrate coupling (16–18), ballistic and diffusive transport processes (11, 19), and rectification (20–22). More recently, noise (23–26), nonlinear response (e.g., negative differential heat conductance), and control by external stimuli (27, 28) have been examined. An important driving factor in this growing interest is the development of experimental capabilities that greatly improve on the ability to gauge temperatures (and “effective” temperatures in nonequilibrium systems) with high spatial and thermal resolutions (29–43) and to infer from such measurement the underlying heat transport processes. In particular, vibrational energy transport/heat conduction in molecular layers and junctions has recently been characterized using different probes (6, 19, 44–52).

The interplay between charge and energy (electronic and nuclear) transport (53–60) is of particular interest as it pertains to the performance of energy-conversion devices, such as thermoelectric, photovoltaic, and electromechanical devices. In particular, the thermoelectric response of molecular junctions, mostly focusing on the junction linear response as reflected by its Seebeck coefficient, has been recently observed (61–65) and theoretically analyzed (2, 20, 64, 66–77). Most of the theoretical work has focused on junctions characterized by coherent electronic

transport in which the electronic and nuclear contribution to heat transport are assumed largely independent of each other. The few recent works that analyze electron–phonon interactions effects on the junction Seebeck coefficient (73, 78–81) do so in the limit of relatively weak electron–phonon interaction (in the sense that the electron is not localized in the junction), using the same level of treatment as applied in the theory of inelastic tunneling spectroscopy.

The present work considers the opposite limit of strong electron–phonon interaction, where electron transport is dominated by successive electron hops subjected to full local thermalization, that is, successive Marcus electron transfer (ET) processes (82–88). By their nature, such successive hops are independent of each other, so a single transfer event may be considered. Even in this well-understood limit different considerations apply under different conditions, and different levels of descriptions were applied to account for the molecular nature of the solvent (89), the dimensionality of the process (90–99), and the definition of the reaction coordinate. Extensions to equilibrium situations have ranged from considerations of deviation from transition state theory (TST) to the description of control by external fields (99–101).

Here, we generalize the standard Marcus (transition state) theory of ET to account for situations where the donor and acceptor sites are characterized by different local temperatures. Such generalization requires the use of multidimensional TST because nuclear polarization modes associated with the different sites are assumed to be equilibrated at their respective local temperatures. Our main results are as follows. (i) We obtain an analytical formula for the ET rate that depends on the two site temperatures and reduces to the standard Marcus form when these temperatures are equal. (ii) The corresponding activation

## Significance

**Electron transfer (ET) is a fundamental process that drives many physical, chemical, and biological transformations, as well as playing a ubiquitous role in the development of technologies for energy conversion and electronics. Recent advances in temperature measurement and control allow thermal gradients and heat flow to be addressed at the molecular level, making it possible to observe electron transfer across thermal gradients. Here, we develop a theory for ET between donor and acceptor sites, where each site has a different local temperature. The transfer of charge across the resulting thermal gradient is found to be coupled with an energy transfer mechanism that may alter heat conduction between sites, even for vanishing net electron current.**

Author contributions: G.T.C. and A.N. designed research, performed research, and wrote the paper.

Reviewers: D.M.L., University of Nevada, Reno; and M.N., Brookhaven National Laboratory.

The authors declare no conflict of interest.

See QnAs on page 9390.

See Commentary on page 9401.

<sup>1</sup>To whom correspondence should be addressed. Email: anitzan@sas.upenn.edu.

 This article contains supporting information online at [www.pnas.org/lookup/suppl/doi:10.1073/pnas.1609141113/-DCSupplemental](http://www.pnas.org/lookup/suppl/doi:10.1073/pnas.1609141113/-DCSupplemental).

energy does not correspond to the geometric activation energy, that is, the point of lowest (free) energy on the isoenergetic surface, and is instead a thermal quantity that depends on the local temperature of each site. (iii) ET between sites of different temperatures is found to be associated with energy transfer between the sites and may affect thermal conduction between sites even when the net electron flux between them vanishes.

We focus on a model that contains the essential ingredients of our theory: The donor and acceptor sites are taken to be at different local temperatures and the ET process is assumed to be dominated by two vibrational modes, one localized near the donor and the other near the acceptor site at the respective local equilibria. Coupling between these modes that is not associated with their mutual coupling to the ET process is disregarded. The ET rate for this bithermal model is obtained and analyzed, along with the implications of this ET process for the energy (heat) transfer between the corresponding sites. Although a general treatment of this problem for systems consisting of large numbers of vibrational modes with associated temperatures is tractable, we defer exposition of this formulation to later work.

### Theory of ET Between Sites of Different Local Temperatures

**Model.** The system under consideration is similar to the model used in Marcus' theory. It comprises two sites, 1 and 2, on which the transferred electron can localize, and the corresponding electronic states are denoted *a* (electron on site 1) and *b* (electron on site 2). The localization is affected by the response of nuclear modes, assumed harmonic, whose equilibrium positions depend on the electronic population. In the implementation of Marcus' theory, this condition is often expressed in terms of a single reaction coordinate; however, the nature of our problem requires the use of at least two groups of modes: one localized near and in (local) thermal equilibrium with site 1 and another localized near and equilibrated with site 2. In the present discussion we consider a minimal model comprising two such modes, denoted  $x_1$  and  $x_2$ , and assume that mode  $x_1$  is sensitive to the temperature and charge on site 1 whereas mode  $x_2$  "feels" the temperature and charging state of site 2. The diabatic electronic (free) energies in states *a* and *b* take the same form as in Marcus' theory (Fig. 1):

$$E_a(x_1, x_2) = E_a^{(0)} + \frac{1}{2}k_1(x_1 - \lambda_1)^2 + \frac{1}{2}k_2x_2^2, \quad [1]$$

$$E_b(x_1, x_2) = E_b^{(0)} + \frac{1}{2}k_1x_1^2 + \frac{1}{2}k_2(x_2 - \lambda_2)^2. \quad [2]$$

In choosing these forms we have taken the equilibrium position of mode  $x_j$ ;  $j \in \{1, 2\}$  to be at the origin when the corresponding site *j* is unoccupied. A schematic of the geometric and energetic properties for ET using the considered multidimensional formalism is shown in Fig. 1C. The reorganization energies for each coordinate are

$$E_{R1} = \frac{1}{2}k_1\lambda_1^2 \quad \text{and} \quad E_{R2} = \frac{1}{2}k_2\lambda_2^2, \quad [3]$$

and the total reorganization energy is

$$E_R = E_{R1} + E_{R2}. \quad [4]$$

As in Marcus' theory, we assume that these modes are in thermal equilibrium with their environments; however, here the environments of sites 1 and 2 are at different local temperatures— $T_1$  and  $T_2$ —and modes  $x_1$  and  $x_2$  are in thermal equilibrium with their corresponding environments. Our aim is to investigate the effect of this thermal nonequilibrium on the ET process and to assess the contribution of the latter to the transport of thermal

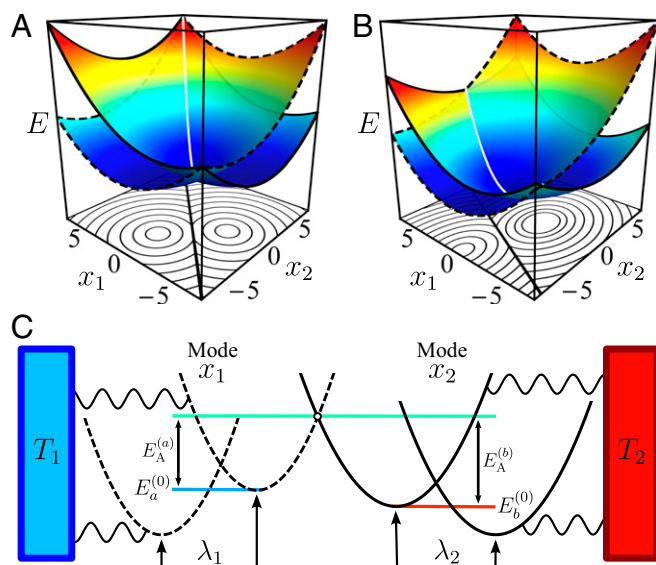


**Fig. 1.** Energy surfaces ( $E_a$  and  $E_b$ ) for ET between (A) symmetric ( $\Delta E_{ba} = 0$ ,  $E_{R1} = E_{R2}$ ) and (B) asymmetric ( $\Delta E_{ba} \neq 0$ ,  $E_{R1} \neq E_{R2}$ ) donor-acceptor pair geometries. The boundary of the  $E_a$  surface is shown dashed and the boundary of the  $E_b$  surface is shown as a solid curve. The *z* axis corresponds to energy *E* and is normalized for visual clarity. Corresponding contour plots are shown below each surface and the CL is shown as a thick black line. (C) Schematic illustration of energy surfaces for ET between modes  $x_1$  (dashed) and  $x_2$  (solid). Each mode is in contact with an independent heat bath. The circular marker denotes a crossing point where  $E_a = E_b$ . In this and all other figures, values are shown in dimensionless reduced units. For convenience, energy may be taken in units of 0.25 eV (a characteristic reorganization energy) and length in units of 1 nm (a characteristic donor-acceptor distance).

energy between the donor and acceptor sites. In considering the latter, we disregard direct coupling between modes localized near the different sites, so that coupling that may lead to energy transfer between such modes can arise only from their mutual interaction with the electronic subsystem. In reality, heat transport between sites occurs also by direct vibrational coupling.

**Multidimensional TST.** Because of large disparity between electronic and nuclear timescales, electronic energy conservation is a condition for an ET event to occur. This implies that such events take place only at nuclear configurations that satisfy  $E_a(x_1, x_2) = E_b(x_1, x_2)$ , which, denoting  $\Delta E_{ba} = E_b^{(0)} - E_a^{(0)}$  and using Eqs. 1 and 2 can be expressed by the condition  $f_c(x_1, x_2) = 0$  where

$$f_c(x_1, x_2) = k_1\lambda_1x_1 - k_2\lambda_2x_2 + \Delta E_{ba} - E_{R1} + E_{R2}. \quad [5]$$

Eq. 5 describes a line in the  $x_1 \times x_2$  space on which the two paraboids displayed in Fig. 1A and B cross. We call this subspace the crossing line (CL).

The Marcus expression for the activation energy is the lowest energy point on this line, and the multidimensional nature of the problem is manifested (in the unithermal case) by an entropic correction to the preexponential factor in the rate expression. Although this level of description is usually adequate, multidimensional variants of Marcus' theory are developed and applied when a reaction proceeds through complex geometric configurations in which multiple reaction pathways are available (97). Zwickl et al. (98) have developed a theory for multiple particle transfer and have also examined to what extent the applicability of a one-dimensional picture persists as the number of intrinsic reaction coordinates is increased. When a charge transfer reaction

occurs through a series of events, a univariate parameterization of the reaction progress must often be replaced by a set of reaction coordinates to adequately describe the mechanism (95). For concerted reaction events, numerical methods developed by Guthrie (96) have extended the parabolic Marcus formalism to quartic energy surfaces in hyperdimensional space. The interplay and competition between sequential and concerted events in ET mechanisms has also been investigated, with Lambert et al. (97) characterizing forbidden and allowed pathways in model systems. As will be seen below, the fact that different modes affected by the ET represent environments of different temperatures has important implications with regard to the multidimensional nature of the transition state.

**Bithermal TST.** Here and below we use the term “bithermal” to refer to a two-mode model in which the different modes are coupled to environments of different temperatures. In classical TST for ET that disregards nuclear tunneling the ET rate from state  $m$  to state  $n$  is

$$k_{m \rightarrow n} = \frac{1}{2} \langle T_m v_{\perp} \rangle P_{m \rightarrow n}, \quad [6]$$

where  $v_{\perp}$  is the velocity in the direction normal to the transition surface,  $P_{m \rightarrow n}$  is the probability density about the transition state on the  $m$  potential surface calculated at the transition state for the  $m \rightarrow n$  process, and  $T_m$  is the tunneling probability in the surface crossing event when coming from the  $m$  side and is a function of  $v_{\perp}$  (102, 103). In the Arrhenius picture, this expression can be interpreted as a product of the frequency of reactive attempts multiplied by the probability that an attempt is successful. Using the Landau–Zener expression for the tunneling probability, we find that  $T_m v_{\perp}$  is a golden-rule type rate that does not depend on  $v_{\perp}$  in the weak coupling (nonadiabatic) limit, and is linear in  $v_{\perp}$  in the strong coupling (adiabatic,  $T_m = 1$ ) limit (*Supporting Information*). For completeness we note that for the two-mode bithermal system considered here, the average velocity in the normal direction is (*Supporting Information*)

$$\langle v_{\perp} \rangle = \sqrt{\frac{4}{\pi} \left( \frac{m_2 \beta_2 k_1 E_{R1} + m_1 \beta_1 k_2 E_{R2}}{|\nabla f_c|^2 m_1 \beta_1 m_2 \beta_2} \right)}, \quad [7]$$

where  $m_j$  is the mass associated with mode  $x_j$  and  $|\nabla f_c|$  is the magnitude of the gradient of the CL constraint. In the unithermal, equal-mass case ( $\beta_1 = \beta_2 = \beta; m_1 = m_2 = m$ ) this expression reduces to the well-known form  $\sqrt{2/\pi m \beta}$ , which is the Boltzmann-weighted expected speed in one dimension (103, 104). Note, however, that donor and acceptor sites with significantly different temperatures are far enough from each other to make the nonadiabatic limit the more relevant.

Next, consider the probability density  $P_{m \rightarrow n}$  to be at the transition surface when moving in the  $m$  electronic state. In the multidimensional version of Marcus theory this probability is given by the standard activation factor  $\exp[-E_A/k_B T]$  ( $k_B$  is Boltzmann’s constant), where the activation energy  $E_A$  is the lowest energy on the transition surface multiplied by a pre-exponential term that can be calculated explicitly (*Supporting Information*). This term will generally also contain entropic corrections that are in the present harmonic model. In the multidimensional–bithermal case, the fact that modes of different temperature are weighted differently on the transition surface has to be taken into account. This is accomplished by using Eqs. 1 and 2 to write the required probability density for electronic state  $a$  as

$$\begin{aligned} P_{a \rightarrow b} &= \iint_{\mathbb{R}^2} |\nabla f_c| e^{-\beta_1 \left(\frac{1}{2} k_1 [x_1 - \lambda_1]^2\right)} e^{-\beta_2 \left(\frac{1}{2} k_2 x_2^2\right)} \\ &\times \delta(f_c(x_1, x_2)) dx_1 dx_2 / \iint_{\mathbb{R}^2} e^{-\beta_1 \left(\frac{1}{2} k_1 [x_1 - \lambda_1]^2\right)} e^{-\beta_2 \left(\frac{1}{2} k_2 x_2^2\right)} dx_1 dx_2 \\ &= \sqrt{\frac{\beta_1 \beta_2 (k_1 E_{R1} + k_2 E_{R2})}{2\pi(\beta_1 E_{R2} + \beta_2 E_{R1})}} \\ &\times \exp \left[ -\beta_1 \beta_2 \frac{(\Delta E_{ba} + E_R)^2}{4(\beta_1 E_{R2} + \beta_2 E_{R1})} \right], \end{aligned} \quad [8]$$

and for electronic state  $b$ ,

$$\begin{aligned} P_{b \rightarrow a} &= \iint_{\mathbb{R}^2} |\nabla f_c| e^{-\beta_1 \left(\frac{1}{2} k_1 x_1^2\right)} e^{-\beta_2 \left(\frac{1}{2} k_2 [x_2 - \lambda_2]^2\right)} \\ &\times \delta(f_c(x_1, x_2)) dx_1 dx_2 / \iint_{\mathbb{R}^2} e^{-\beta_1 \left(\frac{1}{2} k_1 x_1^2\right)} e^{-\beta_2 \left(\frac{1}{2} k_2 [x_2 - \lambda_2]^2\right)} dx_1 dx_2 \\ &= \sqrt{\frac{\beta_1 \beta_2 (k_1 E_{R1} + k_2 E_{R2})}{2\pi(\beta_1 E_{R2} + \beta_2 E_{R1})}} \\ &\times \exp \left[ -\beta_1 \beta_2 \frac{(\Delta E_{ba} - E_R)^2}{4(\beta_1 E_{R2} + \beta_2 E_{R1})} \right], \end{aligned} \quad [9]$$

where  $\beta_j = 1/k_B T_j$ . The factor  $|\nabla f_c|$  renders the constraint  $\delta(f_c(x_1, x_2))$  invariant (105, 106). Intervals of integration  $\mathbb{R}$  and  $\mathbb{R}^2$  denote integration over the regions  $(-\infty, \infty)$  and  $(-\infty, \infty) \times (-\infty, \infty)$ , respectively.

In the relevant nonadiabatic limit, Eqs. 8 and 9 illustrate how the bithermal ET rate is related to the inverse thermal energies  $\beta_1$  and  $\beta_2$  of the respective heat baths. Note that they can be written in the standard forms

$$P_{a \rightarrow b} \propto \exp \left[ -\beta_{\text{eff}} \frac{(\Delta E_{ba} + E_R)^2}{4E_R} \right], \quad [10]$$

$$P_{b \rightarrow a} \propto \exp \left[ -\beta_{\text{eff}} \frac{(\Delta E_{ba} - E_R)^2}{4E_R} \right], \quad [11]$$

with  $\beta_{\text{eff}} = (k_B T_{\text{eff}})^{-1}$ , where the effective temperature is

$$T_{\text{eff}} = T_1 \frac{E_{R1}}{E_R} + T_2 \frac{E_{R2}}{E_R}. \quad [12]$$

An interesting consequence is that in the symmetric case ( $\Delta E_{ba} = 0$ ) the ratio  $P_{a \rightarrow b}/P_{b \rightarrow a} = 1$ , independent of the site temperatures, so the electron is as likely to reside on either the hot or the cold site. In the unithermal limit ( $T_1 = T_2 = T$ ),  $T_{\text{eff}} = T$  and we recover the functional form and temperature dependence predicted by classical Marcus theory (82, 107) (*Supporting Information* contains details of this calculation).

Note that one could naively try to evaluate the ET rates by considering the probability to reach the geometrical barrier, which is the lowest energy point on the transition surface measured relative to the bottom of the reactant surface. The coordinate of this point can be found by minimizing either  $E_a$  or  $E_b$  under the constraint  $E_a = E_b$ . This leads to

$$x_1^{\min} = -\lambda_1 \frac{\Delta E_{ba} - E_R}{2E_R} \quad \text{and} \quad x_2^{\min} = \lambda_2 \frac{\Delta E_{ba} + E_R}{2E_R}. \quad [13]$$

The corresponding geometrical activation energies,  $E_A^{(a)} = E_a(x_1^{\min}, x_2^{\min}) - E_a^{(0)}$  and  $E_A^{(b)} = E_b(x_1^{\min}, x_2^{\min}) - E_b^{(0)}$ , can be cast as additive contributions of energies in mode  $x_1$  and in mode  $x_2$ . Using Eq. 1 we find that for state  $a$

$$E_A^{(a)} = E_{A1}^{(a)} + E_{A2}^{(a)} = \frac{(\Delta E_{ba} + E_R)^2}{4E_R}, \quad [14]$$

where

$$E_{Aj}^{(a)} = E_{Rj} \left( \frac{\Delta E_{ba} + E_R}{2E_R} \right)^2 : j \in \{1, 2\}. \quad [15]$$

Similarly, for state  $b$ ,

$$E_A^{(b)} = E_{A1}^{(b)} + E_{A2}^{(b)} = \frac{(\Delta E_{ba} - E_R)^2}{4E_R}, \quad [16]$$

and

$$E_{Aj}^{(b)} = E_{Rj} \left( \frac{\Delta E_{ba} - E_R}{2E_R} \right)^2 : j \in \{1, 2\}. \quad [17]$$

It follows that the probabilities to reach the configuration  $(x_1^{\min}, x_2^{\min})$  in the  $a$  and  $b$  states satisfy

$$P_{a \rightarrow b} \propto \exp \left[ -(\beta_1 E_{R1} + \beta_2 E_{R2}) \left( \frac{\Delta E_{ba} + E_R}{2E_R} \right)^2 \right] \quad [18]$$

and

$$P_{b \rightarrow a} \propto \exp \left[ -(\beta_1 E_{R1} + \beta_2 E_{R2}) \left( \frac{\Delta E_{ba} - E_R}{2E_R} \right)^2 \right], \quad [19]$$

which are clearly different from Eqs. 8 and 9, although like the latter they go to the Marcus forms in the limit  $\beta_1 = \beta_2$ . Interestingly, Eqs. 18 and 19 can also be written in the forms 8 and 9 but with an effective temperature that satisfies

$$\frac{1}{T_{\text{eff}}} = \frac{1}{T_1} \frac{E_{R1}}{E_R} + \frac{1}{T_2} \frac{E_{R2}}{E_R}, \quad [20]$$

an interesting mismatch with Eq. 12. These differences imply that in the bithermal case the ET rates are no longer controlled by the geometrical barrier.

This can be also seen explicitly: The equal electronic energies condition defines the CL, which can be parametrized in terms of a coordinate  $\alpha$  according to

$$x_1(\alpha) = \frac{k_2 \lambda_2}{k_1 \lambda_1} \alpha + \frac{1}{k_1 \lambda_1} \left( \frac{1}{2} k_1 \lambda_1^2 - \frac{1}{2} k_2 \lambda_2^2 - \Delta E_{ba} \right), \quad [21]$$

$$x_2(\alpha) = \alpha.$$

with a value of the parametric coordinate  $\alpha$  specifying a unique transition point. The energy on the CL,

$$E^\ddagger(\alpha) = E_a[x_1(\alpha), x_2(\alpha)] = E_b[x_1(\alpha), x_2(\alpha)], \quad [22]$$

is parametrized by  $\alpha$ . The energies as a function of position  $\alpha$  on the CL coming from states  $a$  and  $b$ , relative to the corresponding energy origins are

$$E^\ddagger(\alpha) - E_a^{(0)} = \frac{1}{2} k_1 [x_1(\alpha) - \lambda_1]^2 + \frac{1}{2} k_2 [x_2(\alpha)]^2, \quad [23]$$

$$E^\ddagger(\alpha) - E_b^{(0)} = \frac{1}{2} k_1 [x_1(\alpha)]^2 + \frac{1}{2} k_2 [x_2(\alpha) - \lambda_2]^2, \quad [24]$$

respectively. The probabilities to be at point  $\alpha$  on the CL given that we are in the corresponding state satisfy

$$P_{a \rightarrow b}^\ddagger(\alpha) = \frac{e^{-\beta_1 \left( \frac{1}{2} k_1 [x_1(\alpha) - \lambda_1]^2 \right)} e^{-\beta_2 \left( \frac{1}{2} k_2 [x_2(\alpha)]^2 \right)}}{\int_{\mathbb{R}} e^{-\beta_1 \left( \frac{1}{2} k_1 [x_1(\alpha) - \lambda_1]^2 \right)} e^{-\beta_2 \left( \frac{1}{2} k_2 [x_2(\alpha)]^2 \right)} d\alpha}, \quad [25]$$

$$P_{b \rightarrow a}^\ddagger(\alpha) = \frac{e^{-\beta_1 \left( \frac{1}{2} k_1 [x_1(\alpha)]^2 \right)} e^{-\beta_2 \left( \frac{1}{2} k_2 [x_2(\alpha) - \lambda_2]^2 \right)}}{\int_{\mathbb{R}} e^{-\beta_1 \left( \frac{1}{2} k_1 [x_1(\alpha)]^2 \right)} e^{-\beta_2 \left( \frac{1}{2} k_2 [x_2(\alpha) - \lambda_2]^2 \right)} d\alpha}. \quad [26]$$

For  $P_{a \rightarrow b}^\ddagger(\alpha)$ , the point of maximum probability on the CL is found from Eq. 25 to be

$$x_{1,\text{max}}^{(a)} = \frac{\lambda_1 [\beta_2 (-\Delta E_{ba} + E_{R1}) - (\beta_2 - 2\beta_1) E_{R2}]}{2(E_{R2}\beta_1 + E_{R1}\beta_2)}, \quad [27]$$

$$x_{2,\text{max}}^{(a)} = \alpha_{\text{max}}^{(a)} = \frac{\lambda_2 \beta_1 (\Delta E_{ba} + E_R)}{2(E_{R2}\beta_1 + E_{R1}\beta_2)}. \quad [28]$$

A similar procedure using Eq. 26 yields

$$x_{1,\text{max}}^{(b)} = \frac{\lambda_1 \beta_2 (-\Delta E_{ba} + E_R)}{2(E_{R2}\beta_1 + E_{R1}\beta_2)}, \quad [29]$$

$$x_{2,\text{max}}^{(b)} = \alpha_{\text{max}}^{(b)} = \frac{\lambda_2 [\beta_1 (\Delta E_{ba} + E_{R2}) - (\beta_1 - 2\beta_2) E_{R1}]}{2(E_{R2}\beta_1 + E_{R1}\beta_2)}. \quad [30]$$

For  $\beta_1 = \beta_2$ , the position of maximum probability is also the geometric minimum. When the temperatures differ, the position of maximum probability on the transition line shifts from this minimum. The shifts of these probability distributions from their unithermal forms is the reason for the difference between the correct probabilities given by Eqs. 8 and 9, and the forms in Eqs. 18 and 19 obtained under the assumption that the probabilities are dominated by the geometric minimum energy. A graphical representation of these results is shown in Figs. 2 and 3 for several illustrative examples. Fig. 2 shows the position of maximum probability as a function of the temperature difference. The probability densities themselves are shown in Fig. 3. These plots clearly show the essentials of the bithermal transition behavior as discussed above.

The following observations are noteworthy:

- i) The point of maximum probability on the transition surface does not depend on the absolute temperatures  $T_1$  and  $T_2$ , only on their ratios. When  $T_1 = T_2$  it becomes the geometrical point of minimum energy, which is temperature-independent.
- ii) Considering the position of the maximum probability points relative to the minimum energy point on the CL, some general trends can be observed. For reaction free energies below the total reorganization energy ( $|E_{ba}| < E_R$ ) the points of maximum probability in the  $a \rightarrow b$  and  $b \rightarrow a$  directions are on opposite sides of the geometrical energy minimum for  $\beta_2 < \beta_1$ , cross at the unithermal point, and finally continue on opposite sides for  $\beta_2 > \beta_1$ . For reactions with reorganization

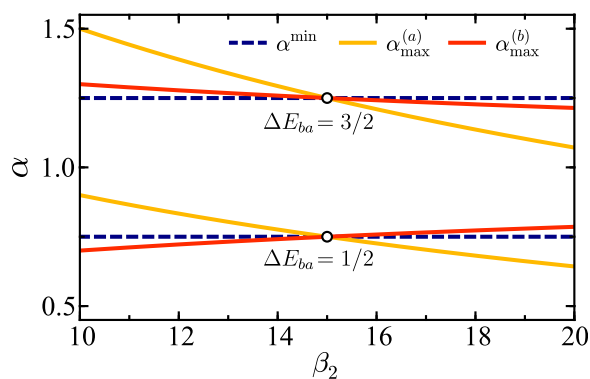


**Fig. 2.** Parametric CL coordinate  $\alpha$  shown as function of  $\beta_2$ , with  $\beta_1 = 15$  held constant, for the geometrical energy minimum (dashed line) and the maximum probability (solid lines) on the  $E_a$  and  $E_b$  surfaces. In the top curves  $\Delta E_{ba} = 3/2$  and in the bottom curves  $\Delta E_{ba} = 1/2$ . The circular markers denote the points where  $\beta_1 = \beta_2$ . Other parameters are  $E_{R1} = E_{R2} = 1/2$ .

energy above the reaction free energy ( $|E_{ba}| > E_R$ ) the maximum probability points for both reaction directions are on same side of the geometrical energy minimum for all values of  $\beta_2$  with  $\beta_1$  held constant, except where they cross at the unithermal point.

- iii) As shown in Fig. 3, in addition to the shift in the transition line probability distribution function, another interesting feature is observed: both the  $P_{a \rightarrow b}^\ddagger$  and  $P_{b \rightarrow a}^\ddagger$  distributions become narrower (smaller variance) with increasing deviation from the unithermal point in the direction  $\beta_1 > \beta_2$  for finite  $\beta_2$  held constant. The inset in each bottom panel of

Fig. 3 illustrates this narrowing as  $\beta_1 \rightarrow \infty$ . In the opposite direction ( $\beta_1 < \beta_2$ ), the complementary trend is observed with the distributions becoming increasingly broad. It is of note that in the limit  $\beta_1 \rightarrow 0$  ( $T_1 \rightarrow \infty$ ) the total distribution will be dominated by the respective distribution of the  $x_2$  coordinate, that is,  $P_{a \rightarrow b}^\ddagger(x_1, x_2) \approx P_{a \rightarrow b}^\ddagger(x_2)$ .

- iv) At the unithermal limit, the maximum probability path that connects stable states is linear and goes through  $\alpha^{\min}$  as shown in Fig. 3. This holds in both the symmetric ( $E_{ba} = 0$ ) and asymmetric cases. In bithermal systems, this path is obviously nonlinear (because it deviates from the minimum energy point) and depends on the thermal characteristics. Fig. 4 demonstrates this observation. Note that unlike in the symmetric case, in an asymmetric system the path connecting minima is not necessarily normal to the CL. This is also the case in unithermal charge transfer reactions with asymmetric donor–acceptor geometry (108). The finding of a thermal energy minimum point that does not correspond to a geometrical energy minimum point is nonintuitive but is congruent with recent advances in TST that have shown that in nonequilibrium systems the traditional picture of a transition state as a stationary saddle point on a potential energy surface is flawed, and that the correct nature is a structure with different extremal properties (109–113).

Finally, an interesting interpretation of the results 8 and 9 can be found in terms of the Tolman activation energy (114), which accounts for statistical properties of the reaction mechanism and goes beyond the Arrhenius viewpoint of a single activation threshold. In the Tolman interpretation, the activation energy is defined as the average energy of all reacting systems minus the average energy of all reactants (114–116). In the present model this is

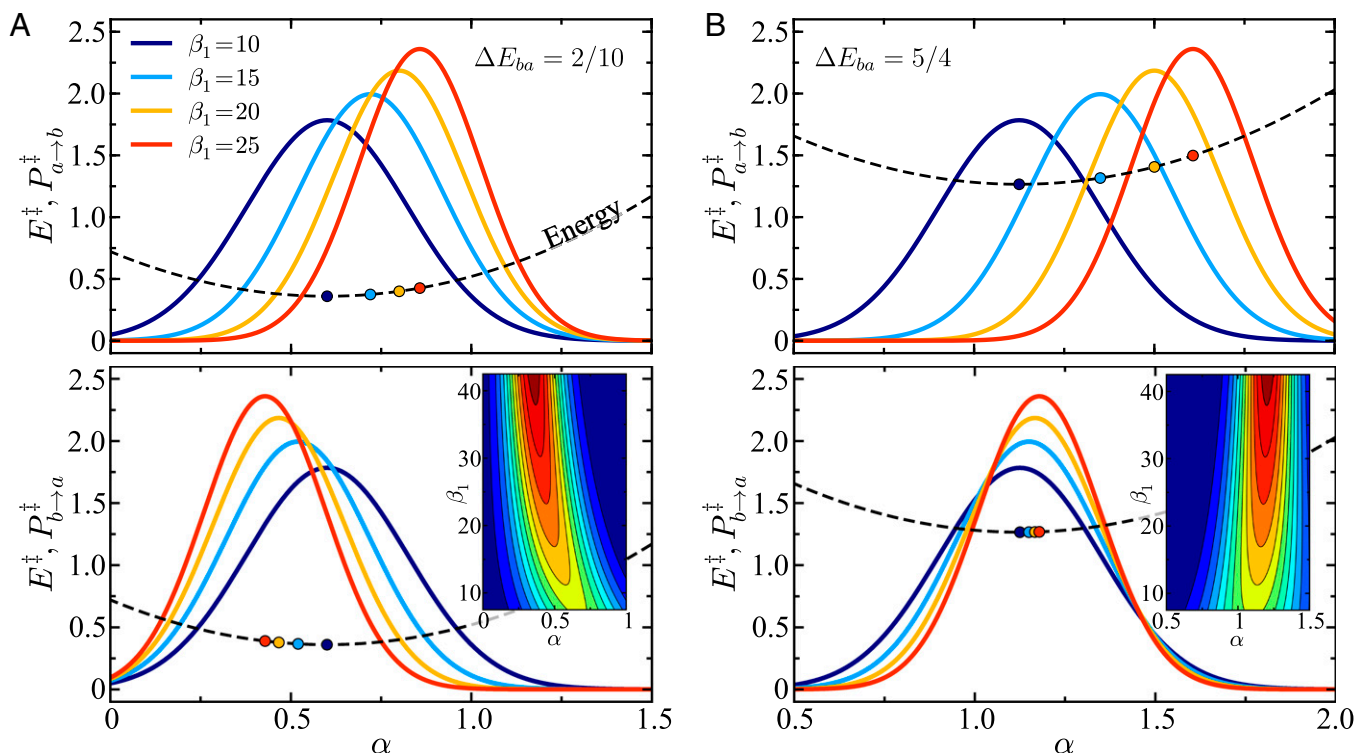


**Fig. 3.** Crossing point probability densities  $P^\ddagger(\alpha)$  for (A)  $\Delta E_{ba} = 2/10$  and (B)  $\Delta E_{ba} = 5/4$  on the  $E_a$  (Top) and  $E_b$  (Bottom) energy surfaces as functions of the CL coordinate  $\alpha$  (Eq. 21). Varying values of  $\beta_1$  are shown with  $\beta_2 = 10$  held constant in all cases. In each panel, the corresponding CL energy  $E^\ddagger$  is shown as a parabolic dashed curve. The circular markers on the energy curves denote the corresponding thermal energy minima (probability density maxima). In each bottom panel, the inset is a corresponding contour plot of  $P_{b \rightarrow a}^\ddagger(\alpha)$  that is normalized with colors varying from blue (minimum) to red (maximum). Other parameters are  $E_{R1} = E_{R2} = 1/2$ .

$$E_A^{\text{Tolman},(m)} = \langle E^\ddagger(\alpha) \rangle_m - E_m^{(0)} : m \in \{a, b\}, \quad [31]$$

where  $E^\ddagger(\alpha)$  is the energy on the CL and the average is over the corresponding distribution ( $m \in \{a, b\}$ ), namely,

$$\langle E^\ddagger(\alpha) \rangle_m = \int_{\mathbb{R}} E^\ddagger(\alpha) P_{m \rightarrow n}^\ddagger(\alpha) d\alpha. \quad [32]$$

Using Eqs. 25 and 26 these averages can be easily evaluated and can be cast as additive terms representing the division of the needed activation energy between modes  $x_1$  and  $x_2$ ,

$$E_A^{\text{Tolman},(m)} = \langle E_{A1}^{(m)} \rangle + \langle E_{A2}^{(m)} \rangle : m \in \{a, b\}, \quad [33]$$

where

$$\begin{aligned} \langle E_{A1}^{(a)} \rangle &= \frac{2\beta_1 E_{R2}^2 + 2\beta_2 E_{R1} E_{R2} + \beta_2^2 E_{R1} (\Delta E_{ba} + E_R)^2}{4(E_{R2}\beta_1 + E_{R1}\beta_2)^2}, \\ \langle E_{A2}^{(a)} \rangle &= \frac{2\beta_2 E_{R1}^2 + 2\beta_1 E_{R1} E_{R2} + \beta_1^2 E_{R2} (\Delta E_{ba} + E_R)^2}{4(E_{R2}\beta_1 + E_{R1}\beta_2)^2}, \\ \langle E_{A1}^{(b)} \rangle &= \frac{2\beta_1 E_{R2}^2 + 2\beta_2 E_{R1} E_{R2} + \beta_2^2 E_{R1} (\Delta E_{ba} - E_R)^2}{4(E_{R2}\beta_1 + E_{R1}\beta_2)^2}, \\ \langle E_{A2}^{(b)} \rangle &= \frac{2\beta_2 E_{R1}^2 + 2\beta_1 E_{R1} E_{R2} + \beta_1^2 E_{R2} (\Delta E_{ba} - E_R)^2}{4(E_{R2}\beta_1 + E_{R1}\beta_2)^2}. \end{aligned} \quad [34]$$

It can be easily checked that defining the probabilities to be on the CL by

$$P_{a \rightarrow b} \propto \exp \left[ -(\beta_1 \langle E_{A1}^{(a)} \rangle + \beta_2 \langle E_{A2}^{(a)} \rangle) \right], \quad [35]$$

and

$$P_{b \rightarrow a} \propto \exp \left[ -(\beta_1 \langle E_{A1}^{(b)} \rangle + \beta_2 \langle E_{A2}^{(b)} \rangle) \right], \quad [36]$$

leads to the exact results 8 and 9 for the bithermal Boltzmann factors. A comparison of rates obtained from the geometrical minimum energy point and the point of maximum probability is shown in Fig. S1 in the Supporting Information.

**Energy Transfer.** As outlined in the introduction, the coupled transfer of charge and heat, and the interplay between the

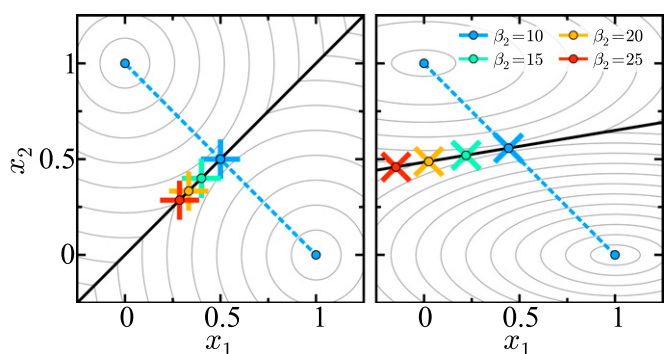


**Fig. 4.** Contour plots of energy surfaces for symmetric (Left) and asymmetric (Right) donor-acceptor pair geometries. The CL is shown as a thick black line. The crosses mark the point of maximum probability for the  $a \rightarrow b$  transition on the CL for  $\beta_2 \in \{10, 15, 20, 25\}$  with  $\beta_1 = 10$  held constant. The dashed line connects the two well minima through the geometrical minimum energy point.

electric and heat currents, gives rise to unique electronic and thermoelectric phenomena (117, 118). When ET takes place across a thermal gradient, it can carry energy as well, implying heat ( $\mathcal{Q}$ ) transfer between the donor and acceptor sites. Indeed, our model has disregarded direct coupling between the modes coupled to the electronic occupation of the different sites, so this coupling is the only potential source (in this model) of heat transfer. Here we explore this possibility.

During the  $m \rightarrow n$  state transition, for mode  $x_j$ , the heat transferred is the sum of the heat released by the corresponding bath during the ascent to the transition state crossing point defined by  $\alpha$  on the  $E_m$  surface, and the heat absorbed by the bath during the descent to equilibrium on the  $E_n$  surface,

$$\mathcal{Q}_j^{(m \rightarrow n)}(\alpha) = -\mathcal{Q}_{\text{rel}}^{(m)} + \mathcal{Q}_{\text{abs}}^{(n)}. \quad [37]$$

For the two-mode, two-state system considered here the amounts of heat transfer into each bath during an ET event are

$$\begin{aligned} \mathcal{Q}_1^{(a \rightarrow b)}(\alpha) &= -\mathcal{Q}_1^{(b \rightarrow a)}(\alpha) \\ &= -\frac{1}{2} k_1 [x_1(\alpha) - \lambda_1]^2 + \frac{1}{2} k_1 [x_1(\alpha)]^2, \\ \mathcal{Q}_2^{(a \rightarrow b)}(\alpha) &= -\mathcal{Q}_2^{(b \rightarrow a)}(\alpha) \\ &= -\frac{1}{2} k_2 [x_2(\alpha)]^2 + \frac{1}{2} k_2 [x_2(\alpha) - \lambda_2]^2. \end{aligned} \quad [38]$$

The signs in Eq. 38 are chosen such that  $\mathcal{Q}$  is positive when energy enters the corresponding bath. The average values for these components are

$$\begin{aligned} \langle \mathcal{Q}_j^{(a \rightarrow b)} \rangle &= \int_{\mathbb{R}} \mathcal{Q}_j^{(a \rightarrow b)}(\alpha) P_{a \rightarrow b}^\ddagger(\alpha) d\alpha, \\ \langle \mathcal{Q}_j^{(b \rightarrow a)} \rangle &= \int_{\mathbb{R}} \mathcal{Q}_j^{(b \rightarrow a)}(\alpha) P_{b \rightarrow a}^\ddagger(\alpha) d\alpha, \end{aligned} \quad [39]$$

where  $j \in \{1, 2\}$  and  $P_{m \rightarrow n}^\ddagger(\alpha)$  is the probability density on the CL for the corresponding surface. Evaluating each of these integrals yields

$$\begin{aligned} \langle \mathcal{Q}_1^{(a \rightarrow b)} \rangle &= \frac{-E_{R1} T_1 \Delta E_{ba} + E_{R1} E_{R2} (T_2 - T_1)}{E_{R1} T_1 + E_{R2} T_2}, \\ \langle \mathcal{Q}_2^{(a \rightarrow b)} \rangle &= \frac{-E_{R2} T_2 \Delta E_{ba} - E_{R1} E_{R2} (T_2 - T_1)}{E_{R1} T_1 + E_{R2} T_2}, \\ \langle \mathcal{Q}_1^{(b \rightarrow a)} \rangle &= \frac{E_{R1} T_1 \Delta E_{ba} + E_{R1} E_{R2} (T_2 - T_1)}{E_{R1} T_1 + E_{R2} T_2}, \\ \langle \mathcal{Q}_2^{(b \rightarrow a)} \rangle &= \frac{E_{R2} T_2 \Delta E_{ba} - E_{R1} E_{R2} (T_2 - T_1)}{E_{R1} T_1 + E_{R2} T_2}, \end{aligned} \quad [40]$$

which depend on the reaction free energy, the reorganization energy in each mode, and the temperature of each bath. It should be emphasized that the modes themselves are assumed to remain in thermal equilibrium. Expressions 40 give the heat transferred into the thermal bath with which the corresponding mode equilibrates for a single ET in the indicated direction. Note that the total heat transfer for the  $a \rightarrow b$  transition is

$$\langle \mathcal{Q}^{(a \rightarrow b)} \rangle = \langle \mathcal{Q}_1^{(a \rightarrow b)} \rangle + \langle \mathcal{Q}_2^{(a \rightarrow b)} \rangle = -\Delta E_{ba}, \quad [41]$$

and correspondingly for the  $b \rightarrow a$  transition,

$$\langle \mathcal{Q}^{(b \rightarrow a)} \rangle = \langle \mathcal{Q}_1^{(b \rightarrow a)} \rangle + \langle \mathcal{Q}_2^{(b \rightarrow a)} \rangle = \Delta E_{ba}, \quad [42]$$

which are just statements of energy conservation. The change in free energy of the baths associated with the  $a \rightarrow b$  process

$(-\Delta E_{ba})$  is divided between the two baths with the ratio  $E_{R1}T_1/E_{R2}T_2$ . Interestingly, this ratio depends on their temperatures, reflecting the fact that the higher-temperature bath is more effective in promoting ET. Even more significant is the observation that there is a term in each expression in 40 that does not depend on  $\Delta E_{ba}$ , and the sign of which does not depend on the direction of the ET process. Thus, there exists a nonzero heat transfer between baths associated with the ET process in bithermal systems. Over each ET event it is given by

$$\langle Q_{2 \rightarrow 1} \rangle \equiv \langle Q_1^{(a \rightarrow b)} \rangle + \langle Q_1^{(b \rightarrow a)} \rangle = \frac{2E_{R1}E_{R2}(T_2 - T_1)}{E_{R1}T_1 + E_{R2}T_2} \quad [43]$$

and

$$\langle Q_{1 \rightarrow 2} \rangle \equiv \langle Q_2^{(a \rightarrow b)} \rangle + \langle Q_2^{(b \rightarrow a)} \rangle = -\frac{2E_{R1}E_{R2}(T_2 - T_1)}{E_{R1}T_1 + E_{R2}T_2}. \quad [44]$$

To see the significance of this result, consider an ensemble of site pairs with probabilities  $p_a$  that a pair is in state  $a$  (electron on site 1) and  $p_b$  that the pair is in state  $b$  (electron on site 2). These probabilities obey the kinetic equations

$$\frac{dp_a}{dt} = -\frac{dp_b}{dt} = -\mathcal{J}_{a \rightarrow b} + \mathcal{J}_{b \rightarrow a}, \quad [45]$$

where  $\mathcal{J}_{a \rightarrow b} = k_{a \rightarrow b}p_a$  and  $\mathcal{J}_{b \rightarrow a} = k_{b \rightarrow a}p_b$ . Correspondingly, the rate of heat deposit on the respective site is given by

$$\frac{dQ_j}{dt} = \mathcal{J}_{a \rightarrow b} \langle Q_j^{(a \rightarrow b)} \rangle + \mathcal{J}_{b \rightarrow a} \langle Q_j^{(b \rightarrow a)} \rangle : j \in \{1, 2\}. \quad [46]$$

Now, consider the steady state at which the system is at electronic quasiequilibrium so that  $\mathcal{J}_{a \rightarrow b} = \mathcal{J}_{b \rightarrow a} = \mathcal{J}_{ss}$ , that is, the net electron flux between sites vanishes. Using Eqs. 43 and 44 it follows that at this state

$$\left( \frac{dQ_1}{dt} \right)_{ss} = -\left( \frac{dQ_2}{dt} \right)_{ss} = \mathcal{J}_{ss} \frac{2E_{R1}E_{R2}(T_2 - T_1)}{E_{R1}T_1 + E_{R2}T_2} \equiv \mathcal{J}_{ss}^Q. \quad [47]$$

Thus, for  $T_1 \neq T_2$ , even when the net electron flux vanishes, the presence of hopping electrons induces a net heat current from the hot bath to the cold bath. Of interest is the observation that there is no pure Seebeck effect in the model investigated here. This is seen in Eqs. 10–12, which imply that when  $E_{R1} = E_{R2}$ , changing  $T_1$  relative to  $T_2$  affects the forward and backward rates in the same way. Note that Eq. 47 is nonlinear in the temperature difference (although it is approximately so when the difference is small). In the high- and low-temperature limits of site 2, the steady-state heat flux becomes

$$\lim_{T_2 \rightarrow \infty} \mathcal{J}_{ss}^Q = 2 \mathcal{J}_{ss} E_{R1} \quad \text{and} \quad \lim_{T_2 \rightarrow 0} \mathcal{J}_{ss}^Q = -2 \mathcal{J}_{ss} E_{R2}, \quad [48]$$

respectively, each of which depends only on the reorganization energy of the respective cold mode. These results imply that in a system where electron hops between local sites there is a contribution to the heat conduction associated with the electronic motion. An assessment of this contribution to the heat conduction in such systems will be made elsewhere.

## Conclusions

A unified theory for the rate and extent of ET and heat transport between bithermal donor–acceptor pairs has been constructed in an augmented Marcus framework. Through application of a multidimensional TST where different modes interact with environments of different temperatures, we have characterized the kinetics of the charge transfer process over various temperature gradients and geometries between reactant and product states. In a bithermal system, the traditional interpretation of the activation energy as a single point derived through geometric minimization of overall points where the donor and acceptor are equienergetic has been shown to not adequately describe the transfer mechanism, and, instead, a statistical interpretation of the activation energy threshold has been developed to account for the biasing of states that arises due to the temperature gradient. We find that entropic rate corrections, which are trivial in the unithermal case, are nontrivial for bithermal systems and are characteristic of the multithermal density of states. Surprisingly, for electron transport across a thermal gradient, the transfer of heat continues to occur even when there is no net transfer of charge. This effect could be harnessed, particularly through molecular junctions and wires (1, 53, 119, 120), to control the transfer of thermal energy in reaction networks with complex systems of heat reservoirs. In turn, the use of these reservoirs to control charge current in thermoelectric systems with nonzero Seebeck coefficients could result in the development of devices and electronics that can be harnessed for application in thermally controlled molecular machines.

A description of the transfer process across smoothly varying temperature gradients and the characterization of possible deviations from the assumed bithermal Boltzmann distribution on the transition state CL are possible areas for future research. The treatment of collective behaviors arising from anharmonic coupling between reactive modes, such as that observed in multiple particle transfer mechanisms (98), will require further characterization of the nature of thermalization (121) and temperature, specifically in systems that are in contact with multiple independent heat baths. The current description gives impetus for experimental verification of the constructed methodologies in bithermal systems.

The bithermal donor–acceptor model considered here can be generalized to systems with multiple reaction pathways. For example, a theoretical description of the transfer mechanism in a donor–bridge–acceptor model can be constructed by extending the dimension of the transition state structure on the crossing “line.” Developing a general description of thermal transition states in ET reactions with many reactive modes could be accomplished through implementation of the geometric transition state formalisms developed for classical reactions in high dimensionality (122). A conjecture supported by the bithermal biasing of the transition state structure predicted here is that multibody temperature gradients can be used to control which reaction pathway is taken in a complex network. The possibility of controlling reactions through multithermally induced deformation of transitions states is a significant finding of this study, and one that is primed for further exploration thorough computation and experiment.

**ACKNOWLEDGMENTS.** This work was supported by the Israel Science Foundation, the US–Israel Binational Science Foundation, and the University of Pennsylvania (A.N.).

- Galperin M, Ratner MA, Nitzan A (2007) Molecular transport junctions: Vibrational effects. *J Phys Condens Matter* 19(10):103201.
- Dubi Y, Di Ventra M (2011) Colloquium: Heat flow and thermoelectricity in atomic and molecular junctions. *Rev Mod Phys* 83(1):131–155.
- Cahill DG, Goodson K, Majumdar A (2002) Thermometry and thermal transport in micro/nanoscale solid-state devices and structures. *J Heat Transfer* 124(2):223–241.
- Cahill DG, et al. (2003) Nanoscale thermal transport. *J Appl Phys* 93(2):793–818.
- Leitner DM (2008) Energy flow in proteins. *Annu Rev Phys Chem* 59(1):233–259.

- Leitner DM (2015) Quantum ergodicity and energy flow in molecules. *Adv Phys* 64(4):445–517.
- Li N, et al. (2012) Colloquium: Phononics: Manipulating heat flow with electronic analogs and beyond. *Rev Mod Phys* 84(3):1045–1066.
- Dhar A (2008) Heat transport in low-dimensional systems. *Adv Phys* 57(5):457–537.
- Luo T, Chen G (2013) Nanoscale heat transfer—from computation to experiment. *Phys Chem Chem Phys* 15(10):3389–3412.

10. Rubtsova NI, Qasim LN, Kurnosov AA, Burin AL, Rubtsov IV (2015) Ballistic energy transport in oligomers. *Acc Chem Res* 48(9):2547–2555.
11. Rubtsova NI, et al. (2015) Room-temperature ballistic energy transport in molecules with repeating units. *J Chem Phys* 142(21):212412.
12. Segal D, Nitzan A, Hänggi P (2003) Thermal conductance through molecular wires. *J Chem Phys* 119(13):6840–6855.
13. Mensah N, Nkrumah G, Mensah S, Allotey F (2004) Temperature dependence of the thermal conductivity in chiral carbon nanotubes. *Phys Lett A* 329(4–5):369–378.
14. Marconnet AM, Panzer MA, Goodson KE (2013) Thermal conduction phenomena in carbon nanotubes and related nanostructured materials. *Rev Mod Phys* 85(3):1295–1326.
15. Al-Ghalith J, Ni Y, Dumitrică T (2016) Nanowires with dislocations for ultralow lattice thermal conductivity. *Phys Chem Chem Phys* 18(15):9888–9892.
16. Chen YC, Zwolak M, Di Ventra M (2005) Inelastic effects on the transport properties of alkanethiols. *Nano Lett* 5(4):621–624.
17. Losego MD, Grady ME, Sottos NR, Cahill DG, Braun PV (2012) Effects of chemical bonding on heat transport across interfaces. *Nat Mater* 11(6):502–506.
18. O'Brien PJ, et al. (2013) Bonding-induced thermal conductance enhancement at inorganic heterointerfaces using nanomolecular monolayers. *Nat Mater* 12(2):118–122.
19. Rubtsova NI, Kurnosov AA, Burin AL, Rubtsov IV (2014) Temperature dependence of the ballistic energy transport in perfluoroalkanes. *J Phys Chem B* 118(28):8381–8387.
20. Segal D (2005) Thermoelectric effect in molecular junctions: A tool for revealing transport mechanisms. *Phys Rev B* 72(16):165426.
21. Wu G, Li B (2007) Thermal rectification in carbon nanotube intramolecular junctions: Molecular dynamics calculations. *Phys Rev B* 76(8):085424.
22. Wu LA, Segal D (2009) Sufficient conditions for thermal rectification in hybrid quantum structures. *Phys Rev Lett* 102(9):095503.
23. Nicolin L, Segal D (2011) Quantum fluctuation theorem for heat exchange in the strong coupling regime. *Phys Rev B* 84(16):161414.
24. Nicolin L, Segal D (2011) Non-equilibrium spin-boson model: Counting statistics and the heat exchange fluctuation theorem. *J Chem Phys* 135(16):164106.
25. Gomez-Solano JR, Petrosyan A, Ciliberto S (2011) Heat fluctuations in a non-equilibrium bath. *Phys Rev Lett* 106(20):200602.
26. Agarwalla BK, Li B, Wang JS (2012) Full-counting statistics of heat transport in harmonic junctions: Transient, steady states, and fluctuation theorems. *Phys Rev E Stat Nonlin Soft Matter Phys* 85(5):051142.
27. Arrachea L, Bode N, von Oppen F (2014) Vibrational cooling and thermoelectric response of nanoelectromechanical systems. *Phys Rev B* 90:125450.
28. Li Q, Duchemin I, Xiong S, Solomon GC, Donadio D (2015) Mechanical tuning of thermal transport in a molecular junction. *J Phys Chem C* 119(43):24636–24642.
29. Huang Z, Xu B, Chen Y, Di Ventra M, Tao N (2006) Measurement of current-induced local heating in a single molecule junction. *Nano Lett* 6(6):1240–1244.
30. Tsutsui M, Taniguchi M, Kawai T (2008) Local heating in metal-molecule-metal junctions. *Nano Lett* 8(10):3293–3297.
31. Hoffmann EA, et al. (2009) Measuring temperature gradients over nanometer length scales. *Nano Lett* 9(2):779–783.
32. Chen R, Wheeler PJ, Di Ventra M, Natelson D (2014) Enhanced noise at high bias in atomic-scale Au break junctions. *Sci Rep* 4(4221):4221.
33. Maher RC, Cohen LF, Le Ru EC, Etchegoin PG (2006) A study of local heating of molecules under surface enhanced Raman scattering (SERS) conditions using the anti-Stokes/Stokes ratio. *Faraday Discuss* 132:77–83, discussion 85–94.
34. Ioffe Z, et al. (2008) Detection of heating in current-carrying molecular junctions by Raman scattering. *Nat Nanotechnol* 3(12):727–732.
35. Ward DR, Corley DA, Tour JM, Natelson D (2011) Vibrational and electronic heating in nanoscale junctions. *Nat Nanotechnol* 6(1):33–38.
36. Dang NC, Bolme CA, Moore DS, McGrane SD (2011) Femtosecond stimulated Raman scattering picosecond molecular thermometry in condensed phases. *Phys Rev Lett* 107(4):043001.
37. Sadat S, Tan A, Chua YJ, Reddy P (2010) Nanoscale thermometry using point contact thermocouples. *Nano Lett* 10(7):2613–2617.
38. Menges F, Riel H, Stemmer A, Gotsmann B (2012) Quantitative thermometry of nanoscale hot spots. *Nano Lett* 12(2):596–601.
39. Lee W, et al. (2013) Heat dissipation in atomic-scale junctions. *Nature* 498(7453):209–212.
40. Desiatov B, Goykhman I, Levy U (2014) Direct temperature mapping of nanoscale plasmonic devices. *Nano Lett* 14(2):648–652.
41. Chen Z, et al. (2015) Imaging local heating and thermal diffusion of nanomaterials with plasmonic thermal microscopy. *ACS Nano* 9(12):11574–11581.
42. Hu Y, Zeng L, Minnich AJ, Dresselhaus MS, Chen G (2015) Spectral mapping of thermal conductivity through nanoscale ballistic transport. *Nat Nanotechnol* 10(8):701–706.
43. Mecklenburg M, et al. (2015) Thermal measurement. Nanoscale temperature mapping in operating microelectronic devices. *Science* 347(6222):629–632.
44. Schwarzer D, Kutne P, Schröder C, Troe J (2004) Intramolecular vibrational energy redistribution in bridged azulene-anthracene compounds: Ballistic energy transport through molecular chains. *J Chem Phys* 121(4):1754–1764.
45. Wang Z, et al. (2007) Ultrafast flash thermal conductance of molecular chains. *Science* 317(5839):787–790.
46. Carter JA, Wang Z, Dlott DD (2008) Spatially resolved vibrational energy transfer in molecular monolayers. *J Phys Chem A* 112(16):3523–3529.
47. Wang Z, et al. (2008) Ultrafast dynamics of heat flow across molecules. *Comput Phys* 350(1–3):31–44.
48. Pein BC, Sun Y, Dlott DD (2013) Controlling vibrational energy flow in liquid alkylbenzenes. *J Phys Chem B* 117(37):10898–10904.
49. Kasyanenko VM, Tesar SL, Rubtsov GI, Burin AL, Rubtsov IV (2011) Structure dependent energy transport: Relaxation-assisted 2DIR measurements and theoretical studies. *J Phys Chem B* 115(38):11063–11073.
50. Meier T, et al. (2014) Length-dependent thermal transport along molecular chains. *Phys Rev Lett* 113(6):060801.
51. Kurnosov AA, Rubtsov IV, Burin AL (2015) Communication: Fast transport and relaxation of vibrational energy in polymer chains. *J Chem Phys* 142(1):011101.
52. Yue Y, et al. (2015) Band-selective ballistic energy transport in alkane oligomers: toward controlling the transport speed. *J Phys Chem B* 119(21):6448–6456.
53. Galperin M, Nitzan A, Ratner MA (2007) Heat conduction in molecular transport junctions. *Phys Rev B* 75(15):155312.
54. Galperin M, Saito K, Balatsky AV, Nitzan A (2009) Cooling mechanisms in molecular conduction junctions. *Phys Rev B* 80(11):115427.
55. Galperin M, Nitzan A (2011) Raman scattering and electronic heating in molecular conduction junctions. *J Phys Chem Lett* 2(17):2110–2113.
56. Galperin M, Nitzan A (2011) Raman scattering from biased molecular conduction junctions: The electronic background and its temperature. *Phys Rev B* 84(19):195325.
57. Horsfield AP, et al. (2006) The transfer of energy between electrons and ions in solids. *Rep Prog Phys* 69(4):1195–1234.
58. D'Agosta R, Di Ventra M (2008) Local electron and ionic heating effects on the conductance of nanostructures. *J Phys Condens Matter* 20(37):374102.
59. Asai Y (2011) Theory of local heating in single molecular bridge junctions. *Phys Rev B* 84(8):085436.
60. Asai Y (2015) Vibronic spectroscopy using current noise. *Phys Rev B* 91(16):161402.
61. Reddy P, Jang SY, Segalman RA, Majumdar A (2007) Thermoelectricity in molecular junctions. *Science* 315(5818):1568–1571.
62. Malen JA, et al. (2009) The nature of transport variations in molecular hetero-junction electronics. *Nano Lett* 9(10):3406–3412.
63. Malen JA, Yee SK, Majumdar A, Segalman RA (2010) Fundamentals of energy transport, energy conversion, and thermal properties in organic-inorganic hetero-junctions. *Chem Phys Lett* 491(4–6):109–122.
64. Tan A, et al. (2011) Effect of length and contact chemistry on the electronic structure and thermoelectric properties of molecular junctions. *J Am Chem Soc* 133(23):8838–8841.
65. Kim Y, Jeong W, Kim K, Lee W, Reddy P (2014) Electrostatic control of thermoelectricity in molecular junctions. *Nat Nanotechnol* 9(11):881–885.
66. Paulsson M, Datta S (2003) Thermoelectric effect in molecular electronics. *Phys Rev B* 67(24):241403.
67. Koch J, von Oppen F, Oreg Y, Sela E (2004) Thermopower of single-molecule devices. *Phys Rev B* 70(19):195107.
68. Pauly F, Viljas JK, Cuevas JC (2008) Length-dependent conductance and thermopower in single-molecule junctions of dithiolated oligophenylene derivatives: A density functional study. *Phys Rev B* 78(3):035315.
69. Bergfield JP, Stafford CA (2009) Thermoelectric signatures of coherent transport in single-molecule heterojunctions. *Nano Lett* 9(8):3072–3076.
70. Bergfield JP, Solis MA, Stafford CA (2010) Giant thermoelectric effect from transmission supernodes. *ACS Nano* 4(9):5314–5320.
71. Ke SH, Yang W, Curtarolo S, Baranger HU (2009) Thermopower of molecular junctions: An ab initio study. *Nano Lett* 9(3):1011–1014.
72. Liu YS, Chen YC (2009) Seebeck coefficient of thermoelectric molecular junctions: First-principles calculations. *Phys Rev B* 79(19):193101.
73. Ren J, Zhu JX, Gubernatis JE, Wang C, Li B (2012) Thermoelectric transport with electron-phonon coupling and electron-electron interaction in molecular junctions. *Phys Rev B* 85(15):155443.
74. Wang Y, Zhou J, Yang R (2011) Thermoelectric properties of molecular nanowires. *J Phys Chem C* 115(49):24418–24428.
75. Lee ES, Cho S, Lyeo HK, Kim YH (2014) Seebeck effect at the atomic scale. *Phys Rev Lett* 112(13):136601.
76. Amanatidis I, Kao JY, Du LY, Pao CW, Chen YC (2015) Thermoelectric efficiency of single-molecule junctions: Phase diagram constructed from first-principles calculations. *J Phys Chem C* 119(52):28728–28736.
77. Simine L, Chen WJ, Segal D (2015) Can the Seebeck coefficient identify quantum interference in molecular conduction? *J Phys Chem C* 119(22):12097–12108.
78. Walczak K (2007) Thermoelectric properties of vibrating molecule asymmetrically connected to the electrodes. *Physica B* 392(1–2):173–179.
79. Koch T, Loos J, Fehske H (2014) Thermoelectric effects in molecular quantum dots with contacts. *Phys Rev B* 89(15):155133.
80. Perroni CA, Ninno D, Cataudella V (2014) Electron-vibration effects on the thermoelectric efficiency of molecular junctions. *Phys Rev B* 90(12):125421.
81. Zimbovskaya NA (2014) The effect of dephasing on the thermoelectric efficiency of molecular junctions. *J Phys Condens Matter* 26(27):275303.
82. Marcus RA (1956) On the theory of oxidation-reduction reactions involving electron transfer. I. *J Chem Phys* 24(5):966–978.
83. Marcus RA (1964) Chemical and electrochemical electron-transfer theory. *Annu Rev Phys Chem* 15(1):155–196.
84. Marcus RA, Sutin N (1985) Electron transfers in chemistry and biology. *Biochim Biophys Acta* 811(3):265–322.
85. Marcus RA (1993) Electron transfer reactions in chemistry. Theory and experiment. *Rev Mod Phys* 65:599–610.
86. Tachiya M (1993) Generalization of the Marcus equation for the electron-transfer rate. *J Phys Chem* 97(22):5911–5916.
87. Nitzan A (2006) *Chemical Dynamics in Condensed Phases: Relaxation, Transfer and Reactions in Condensed Molecular Systems* (Oxford Univ Press, Oxford).
88. Peters B (2015) Common features of extraordinary rate theories. *J Phys Chem B* 119(21):6349–6356.

89. Zichi DA, Ciccotti G, Hynes JT, Ferrario M (1989) Molecular dynamics simulation of electron-transfer reactions in solution. *J Phys Chem* 93(17):6261–6265.
90. Tachiya M (1989) Relation between the electron-transfer rate and the free energy change of reaction. *J Phys Chem* 93(20):7050–7052.
91. Steeger M, et al. (2015) On the relation of energy and electron transfer in multidimensional chromophores based on polychlorinated triphenylmethyl radicals and triarylamines. *Phys Chem Chem Phys* 17(17):11848–11867.
92. Soudackov AV, Hazra A, Hammes-Schiffer S (2011) Multidimensional treatment of stochastic solvent dynamics in photoinduced proton-coupled electron transfer processes: Sequential, concerted, and complex branching mechanisms. *J Chem Phys* 135(14):144115.
93. Hammes-Schiffer S (2015) Proton-coupled electron transfer: Moving together and charging forward. *J Am Chem Soc* 137(28):8860–8871.
94. Harshan AK, Yu T, Soudackov AV, Hammes-Schiffer S (2015) Dependence of vibronic coupling on molecular geometry and environment: Bridging hydrogen atom transfer and electron-proton transfer. *J Am Chem Soc* 137(42):13545–13555.
95. Grunwald E (1985) Structure-energy relations, reaction mechanism, and disparity of progress of concerted reaction events. *J Am Chem Soc* 107(1):125–133.
96. Guthrie JP (1996) Multidimensional Marcus theory: An analysis of concerted reactions. *J Am Chem Soc* 118(51):12878–12885.
97. Lambert C, Nöll G, Hampel F (2001) Multidimensional electron transfer pathways in a tetrahedral tetrakis phosphonium salt: One-step vs two-step mechanism. *J Phys Chem A* 105(32):7751–7758.
98. Zwickl J, Shenvi N, Schmidt JR, Tully JC (2008) Transition state barriers in multidimensional Marcus theory. *J Phys Chem A* 112(42):10570–10579.
99. Rubtsov IV (2015) State-specific electron transfer: Shake it off. *Nat Chem* 7(9):683–684.
100. Delor M, Sazanovich IV, Towrie M, Weinstein JA (2015) Probing and exploiting the interplay between nuclear and electronic motion in charge transfer processes. *Acc Chem Res* 48(4):1131–1139.
101. Delor M, et al. (2015) On the mechanism of vibrational control of light-induced charge transfer in donor-bridge-acceptor assemblies. *Nat Chem* 7(9):689–695.
102. Hammes-Schiffer S, Tully JC (1995) Nonadiabatic transition state theory and multiple potential energy surface molecular dynamics of infrequent events. *J Chem Phys* 103(19):8528–8537.
103. Jóhannesson GH, Jónsson H (2001) Optimization of hyperplanar transition states. *J Chem Phys* 115(21):9644–9656.
104. Voth GA, Chandler D, Miller W (1989) Rigorous formulation of quantum transition state theory and its dynamical corrections. *J Chem Phys* 91(12):7749.
105. Vanden-Eijnden E, Tal FA (2005) Transition state theory: Variational formulation, dynamical corrections, and error estimates. *J Chem Phys* 123(18):184103.
106. Hartmann C, Latorre JC, Ciccotti G (2011) On two possible definitions of the free energy for collective variables. *Eur Phys J Spec Top* 200(1):73–89.
107. Richardson JO, Thoss M (2014) Non-oscillatory flux correlation functions for efficient nonadiabatic rate theory. *J Chem Phys* 141(7):074106.
108. Newton MD (2015) Extension of Hopfield's electron transfer model to accommodate site-site correlation. *J Phys Chem B* 119(46):14728–14737.
109. Bartsch T, Hernandez R, Uzer T (2005) Transition state in a noisy environment. *Phys Rev Lett* 95(5):058301.
110. Craven GT, Bartsch T, Hernandez R (2014) Persistence of transition-state structure in chemical reactions driven by fields oscillating in time. *Phys Rev E Stat Nonlin Soft Matter Phys* 89(4):040801.
111. Craven GT, Bartsch T, Hernandez R (2014) Communication: Transition state trajectory stability determines barrier crossing rates in chemical reactions induced by time-dependent oscillating fields. *J Chem Phys* 141(4):041106.
112. Craven GT, Bartsch T, Hernandez R (2015) Chemical reactions induced by oscillating external fields in weak thermal environments. *J Chem Phys* 142(7):074108.
113. Craven GT, Hernandez R (2015) Lagrangian descriptors of thermalized transition states on time-varying energy surfaces. *Phys Rev Lett* 115(14):148301.
114. Tolman RC (1920) Statistical mechanics applied to chemical kinetics. *J Am Chem Soc* 42(12):2506–2528.
115. Truhlar DG (1978) Interpretation of the activation energy. *J Chem Educ* 55(5):309.
116. Truhlar D, Kohen A (2001) Convex Arrhenius plots and their interpretation. *Proc Natl Acad Sci USA* 98(3):848–851.
117. Esposito M, Ochoa MA, Galperin M (2015) Efficiency fluctuations in quantum thermoelectric devices. *Phys Rev B* 91(11):115417.
118. Lim JS, López R, Sánchez D (2013) Dynamic thermoelectric and heat transport in mesoscopic capacitors. *Phys Rev B* 88:201304.
119. Schiff PR, Nitzan A (2010) Kramers barrier crossing as a cooling machine. *Chem Phys* 375(2–3):399–402.
120. Chtchelkatchev NM, Glatz A, Beloborodov IS (2013) Interplay of charge and heat transport in a nano-junction in the out-of-equilibrium cotunneling regime. *J Phys Condens Matter* 25(18):185301.
121. Popov AV, Hernandez R (2007) Ontology of temperature in nonequilibrium systems. *J Chem Phys* 126(24):244506.
122. Uzer T, Jaffé C, Palacián J, Yanguas P, Wiggins S (2002) The geometry of reaction dynamics. *Nonlinearity* 15(4):957–992.
123. Thompson DL (1998) *Modern Methods for Multidimensional Dynamics Computations in Chemistry* (World Scientific, Singapore).
124. Lykhin AO, Kaliakin DS, dePolo GE, Kuzubov AA, Varganov SA (2016) Nonadiabatic transition state theory: Application to intersystem crossings in the active sites of metal-sulfur proteins. *Int J Quantum Chem* 116(10):750–761.
125. Menzinger M, Wolfgang R (1969) The meaning and use of the Arrhenius activation energy. *Angew Chem Int Ed* 8(6):438–444.
126. Kohen A, Cannio R, Bartolucci S, Klinman JP (1999) Enzyme dynamics and hydrogen tunnelling in a thermophilic alcohol dehydrogenase. *Nature* 399(6735):496–499.